An Adaptive Solar Photovoltaic Array Using Model-Based Reconfiguration Algorithm

Dzung Nguyen, *Student Member, IEEE*, and Brad Lehman, *Member, IEEE*

***Abstract*—This paper proposes an adaptive reconfiguration scheme to reduce the effect of shadows on solar panels. A switching matrix connects a solar adaptive bank to a fixed part of a solar photovoltaic (PV) array, according to a model-based control algorithm that increases the power output of the solar PV array. Control algorithms are implemented in real time. An experimental reconfiguration PV system with a resistive load is presented and is shown to verify the proposed reconfigurations.**

***Index Terms*—Adaptive, model based, photovoltaic (PV), reconfiguration.**

NOMENCLATURE

I_{A_j}	Photo-generated current of solar cells in the adaptive bank.
$V_{\mathrm{OC}A_j}$	Open-circuit voltage of solar cell A_j.
R_{SH}	Shunt resistance of a solar cell, submodule.
I_S	Saturation current of a solar cell diode.
A	Ideality factor of a solar cell.
K	Boltzman's constant.
T	Cell operating temperature.
Q	Electron charge.
I_{F_j}	Photo-generated current of submodules in a fixed part.
V_j	Voltages of submodules.
I_{out}	Output current of a solar array.
R_{SM}	Series resistance of a solar cell, submodule.
R_{SHM}	Shunt resistance of a solar cell, module.
n	Number of solar cells in a submodule.

I. INTRODUCTION

MASS PRODUCTION and use of electricity generated from solar energy has recently become more common, perhaps because of the environmental threats arising from the production of electricity from fossil fuels and nuclear power. However, in many applications, such as solar power plants, building integrated photovoltaic (PV), or solar tents, solar PV arrays might be illuminated nonuniformly.

The cause of nonuniform illumination may be shadows from clouds, trees, booms, neighbor's houses, or even the shadow of one solar array on the other, etc. For example, Fig. 1(a) shows a portable flexible solar array that is embedded into fabric. These new-generation solar arrays can be folded and carried by campers and soldiers to remote locations. Often, they are left alone to charge batteries near trees and fences and have been reported to even be wrapped around telephone poles or trees [1]–[3].

(a) (b)

Fig. 1. Shadow configurations. (a) Shadow on portable solar array. (b) Shadow from one array cast on another array.

Furthermore, for applications like BIPV and solar power plants in small spaces, as shown in Fig. 1(b), shadows from one solar PV array are commonly cast on another array [4], [5]. In conventional solar PV plants, the designer must solve the complex problem, i.e., the tradeoff between "maximum energy output" and "minimum produced energy cost," by varying the distance between the rows [4].

For these new applications, it has been particularly important to optimize the performance of the arrays in shadowed conditions.

Because of the nature of the electrical characteristics of solar cells, the maximum power losses are not proportional to the shadow but magnify nonlinearly [2]. The shadow of a solar PV array can cause many undesired effects, including the following.

1) The real power generated from the solar PV array is much less than designed so that the loss of load probability increases [6].
2) The local hot spot in the shaded part of the solar PV array can damage the solar cells [7].

There are several approaches that have been proposed to reduce the effect of shadows on a solar PV array's output power.

1) Bypass diodes are connected across shadowed cells to pass the full amount of current while preventing damage to the solar cell [7], [8]. This method usually requires a great number of bypass diodes that are integrated in the solar arrays. The production of solar arrays with bypass diodes is more costly. Furthermore, the power losses of solar PV arrays are not completely prevented because there are additional power losses when the current passes though the bypass diodes.
2) In large systems, each of the solar submodules can be connected to its own maximum power point (MPP) tracking dc–dc converter and can individually operate near

Manuscript received October 15, 2007; revised April 7, 2008. This work was supported in part by a grant from the Vietnam Education Foundation (VEF).

The authors are with Northeastern University, Boston, MA 02115 USA (e-mail: nguyen.dun@ neu.edu; lehman@ece.neu.edu).

Color versions of one or more of the figures in this paper are available online at http://ieeexplore.ieee.org.

Digital Object Identifier 10.1109/TIE.2008.924169

its own MPP. Thus, the efficiency of the whole system is increased [9]–[12], but the method requires a large number of dc–dc converters (equal to the number of solar modules).

3) An alternate research field, which is also the focus of this paper, is one that adaptively reconfigures solar array connections in real time in order to track maximum output power. Traditionally, fixed solar PV arrays have hard-wired interconnections between their solar cells. These connections are not changed after installation. However, it is possible to continuously rearrange solar cells in series and parallel connections [13] to facilitate the PV system to work more as a constant power source, even in different operating conditions (i.e., insolation, temperature, loads, etc.). Research studies in [14]–[16] have started to develop methods to reconfigure solar cells to improve power output in shaded conditions. This research [15], [16] focuses mostly on how to build the arrays and does not propose real-time executable control algorithms (the focus of this paper). Because of this, the proposed methods have an unrealistic number of sensors and switches that must use complex control algorithms to determine when it turns the switch on or off [15], [16].

This paper develops research for the third approach. Adaptive reconfiguration of solar arrays is proposed, which requires significantly fewer voltages or current sensors and switches than in [15] and [16]. Further, as published for the first time, simple real-time executable control algorithms that determine how to adaptively reconfigure solar cell connections have been developed. The algorithms have been experimentally tested on a small-scale solar reconfiguration system.

Specifically, this paper presents the following research contributions.

1) A new method for reconfiguration of solar PV arrays in real time under shadow conditions is presented. Solar cells from a (smaller) solar adaptive bank will be connected to the (larger) fixed part of the solar array. The MPP of the whole array is tracked by a single common MPP tracker (MPPT), instead of many MPPTs, as shown in [9]–[12]. Since only a small percentage of the solar arrays are reconfigurable, fewer switches and simplified control algorithms are possible. In the uniform illumination conditions, all these adaptive solar cells will be equally connected to all rows of the fixed part of the solar PV array. In nonuniform illumination conditions, the number of the adaptive solar cells connected to the shaded submodules depends on the shaded area of the submodules. The reconfiguration is executed through the proposed switching matrix.
2) Simple control decision algorithms are presented to determine when and how to open and close switches between the fixed part and adaptive bank of the solar PV array. The algorithms rely on model predictions that can be implemented in real time by microcontrollers or digital signal processors.

An experimental adaptively reconfigurable solar PV array has been built and tested to verify the proposed reconfigurations. It is shown that the proposed approach is able to increase the output power of the solar PV array in real time under shaded conditions by 30% for a typical experiment.

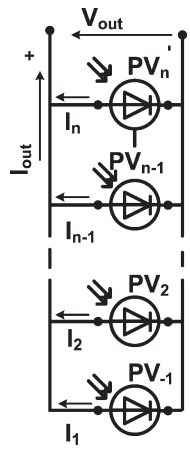

Fig. 2. Parallel connection.

II. Solar Cells Connection and the Shadow Problem

A. Parallel Connection

Fig. 2 shows that solar cells $\mathrm{PV}_1, \mathrm{PV}_2, \ldots, \mathrm{PV}_n$ are connected in parallel to create the solar submodule. The output current is equal to the sum of the currents of all the solar cells, i.e.,

$$I_{\text{out}} = \sum_{i=1}^{n} I_i. \tag{1}$$

The output voltage is equal to the voltage in each of the solar cells, i.e.,

$$V_{\text{out}} = V_1 = \cdots = V_n. \tag{2}$$

The output power of the solar submodule is given by

$$P_{\text{out}} = I_{\text{out}} \times V_{\text{out}} = V_{\text{out}} \times \sum_{i=1}^{n} I_i = \sum_{i=1}^{n} P_i. \tag{3}$$

A single shadow over a solar cell does not affect the power delivered by the other solar cells in the submodule. Thus, it is the most robust configuration for a solar array under shadow conditions. However, the output voltage is very low ($\sim$0.5 V).

B. Series Connection

A solar cell has a very low output voltage, which is around 0.5 V. To create a higher dc output voltage, solar cells PV_1, $\mathrm{PV}_2, \ldots, \mathrm{PV}_{m-1}, \mathrm{PV}_m$ are often connected in series, as shown in the parallel connection in Fig. 3. The output voltage and output power of the string of the series-connected solar cells is

$$V_{\text{out}} = \sum_{i=1}^{n} V_i \tag{4}$$

$$P_{\text{out}} = I_{\text{out}} \times V_{\text{out}}. \tag{5}$$

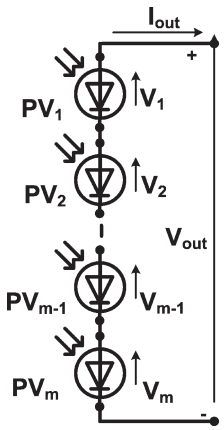

Fig. 3. Series connection.

All the solar cells share the same current, denoted by $I_{\rm out}$. Thus, when one solar cell becomes shaded, it directly affects the power delivered by the other cells. That is, $I_{\rm out}$ decreases throughout all the cells, and there is a significant power drop.

C. Different Configurations of Solar PV Arrays and the Maximum Power Losses of the Shadow

Fig. 4 shows the two common solar PV array configurations that utilize the combinations of the connections. In this figure, each $\mathrm{PV}_{(i,j)}$ is an individual solar cell.

The solar cells are connected in series and parallel to create a solar array.

1) *Simple series–parallel (SP) array:* when all solar cells, for example, $\mathrm{PV}_{1,1}, \mathrm{PV}_{2,1}, \ldots, \mathrm{PV}_{m-1,1}, \mathrm{PV}_{m,1}$, are connected in series, creating strings. Then, all these strings are connected in parallel, as shown in Fig. 4(a).
2) *Total-cross-tied (TCT) array:* when all solar cells are connected in parallel, for example, $\mathrm{PV}_{1,1}, \mathrm{PV}_{1,2}, \ldots, \mathrm{PV}_{1,n-1}, \mathrm{PV}_{1,n}$, creating modules. Then, these modules are connected in series, as shown in Fig. 4(b).

Fig. 5 shows a typical result of calculation of the power losses for SP and TCT for an array with 100 solar cells.

For an SP connection, each solar cell in a different column completely shaded can cause up to a 10% extra loss when shaded. The percent of lost power depends on nonlinear functions, as described in Section III. For example, if six solar cells from different columns are completely shaded, the estimated power loss in Fig. 5 (point A) will be around 48%. On the other hand, if the six cells are in three different columns, then the power loss (point B) is reduced to about 17%. For a TCT connection, each solar cell in the same row completely shaded can cause up to a 10% extra power loss. If two cells in different rows are shaded, then the power loss is the same as one row being shaded. Referring to Fig. 5 again, when the six solar cells in the same row completely shaded, then the power loss of the array is around 48% (point A). If the six shaded cells have only three shaded cells in the same row, then the power loss is about 17% (point B).

In the worst case of ten fully shaded solar cells (10% of the total number of solar cells in the solar PV array), the maximum output power can be reduced by more than 90%. The result is the same for both SP and TCT.

III. Proposed Adaptive Reconfiguration Method

This section proposes a system architecture that permits adaptive reconfiguration of the connections between solar PV arrays. A switching matrix that connects a small reconfigurable bank of PV arrays with a larger nonreconfigurable bank of solar PV arrays is proposed. Because only the adaptive bank is being reconfigured, the number of switches and reconfiguration time seems computationally efficient. We propose two different adaptive reconfiguration algorithms for the arrays, each of which will eventually produce the same increase in power under shadow conditions. The first method is simpler, and it relies on a serial "bubble-sort" approach, which switches the adaptive PV arrays one at a time. After each switching, the power of the total system is analyzed, and the next sort is implemented. In the second method, a model reference approach that is able to predict power levels in each of the rows of the fixed solar arrays and uses this prediction to simultaneously switch the connections of the adaptive bank is proposed.

These reconfiguration control algorithms are applicable, even when some of the solar cells of the adaptive PV bank are shaded: The control algorithms will automatically connect the most illuminated solar cells in the adaptive bank to the most shaded row of the fixed part. If a solar cell in the adaptive bank is shaded, it will still be connected to the fixed solar array, perhaps to a more illuminated row. Since there is a parallel connection, the only implication is that there will only be a small amount of current/power added from the shaded adaptive solar cell. In either case, the two different approaches will eventually produce the same increased power of the entire solar PV system, and both are implementable on a digital signal processor in real time. However, the second approach is quicker, as we later demonstrate experimentally.

Fig. 6 shows the operation principle of the proposed method.

Fixed Part (m Rows and n Columns): The fixed part is the main part of the solar array and has the most number of solar cells, as shown in Fig. 6. The fixed part contains $m \times n$ solar cells [i.e., solar cells $(1,1), (1,2), \ldots (m, n-1), (m,n)$]. All solar cells in the fixed part are hardwired and have a fixed configuration, with a TCT interconnection. We can consider that the fixed part of the solar PV array has m PV "modules" connected in series.

Solar Adaptive Bank of Solar Cells: In this paper, the adaptive bank has m solar cells (i.e., solar cells $A_1, A_2, \ldots, A_m$) not connected together, i.e., the number of adaptive solar cells is the same as the number of rows in the fixed part. These adaptive solar cells can be connected in parallel to any PV module, from PV_1 to PV_m, as seen in Fig. 6. We remark that fewer than m adaptive solar cells can also be used. (The algorithms still work, and there will still be power improvement after reconfiguration, as shown in Section IV). However, by selecting m adaptive solar cells, there is the advantage that when there is uniform illumination and there is no need for reconfiguration, the adaptive bank can form one additional column to the fixed part.

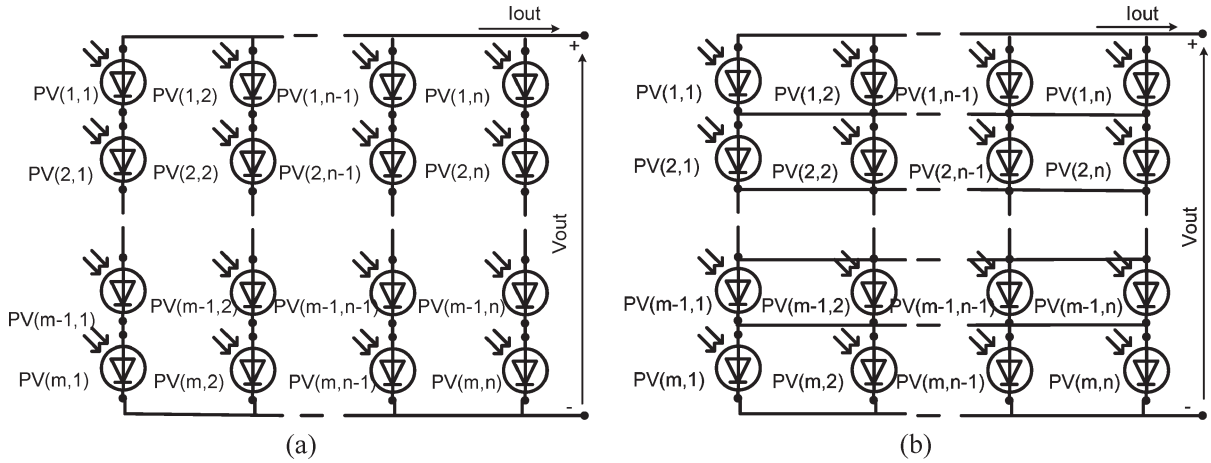

Fig. 4. Solar PV array's common interconnections. (a) SP interconnection. (b) TCT interconnection.

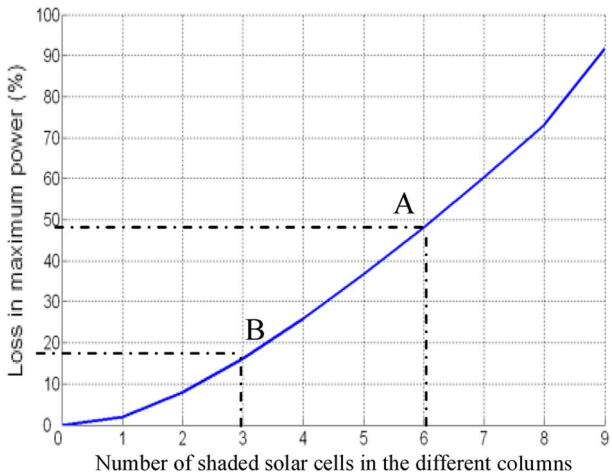

Fig. 5. Losses of maximum power depend on the shaded area. In SP, one cell in each column is fully shaded. In TCT, one cell in the same row is fully shaded.

In this case, the entire PV system will behave like an $m \times (n+1)$ array.

Switching Matrix: The fixed part and the solar adaptive bank are connected together through the switching matrix. The switching matrix, as shown in Fig. 7, contains switches $S(1,1)$, $S(1,2),\ldots,S(m-1,m-1),S(m,m)$ connect each solar cell in the adaptive bank to any row of solar cells in the fixed part of the PV array. When the switch $S(i,j)$ is on, the solar cell A_i from the adaptive bank will be connected to row j of a fixed part. Thus, only one set of switches in a column can be on at a time. The switches can either be relays or electrical switches. In the proposed method, each switch carries just the current of one solar cell (or one submodule), which is normally 1–5 A, even for large solar power plants. Thus, if mechanical relays are selected, the arcing phenomena may not be burdensome since the current is so low. On the other hand, small electrical switches (in SO8 packages) are made at suitable power and voltage ratings for applications such as those in Fig. 1(a). Furthermore, these small package sizes are easily embedded/sewn into the fabric. Therefore, it seems that these portable foldable solar panels are prime candidates for this reconfiguration approach.

"Bubble-Sort" Method: The flowchart of the "bubble-sort" method is shown in Fig. 8(a). In general, the solar array is reconfigured by the following principle: If the voltage of one row is smaller than the voltages of the other rows, it indicates that this row is the most shaded row. One solar cell from the adaptive bank will be switched in parallel to this row. The process will continue until all the solar cells of the solar adaptive bank are connected in parallel to the rows of the fixed part.

Step 1) The solar adaptive bank and the fixed part of the solar array are connected together in the original configuration, as in Fig. 9(a). Voltages V_1 and V_{out} are monitored, where V_1 is the voltage produced by row 1 of the solar array. In the uniform illumination, we define the output voltage as follows: $V_{\text{out}} = m \times V_1$. In the nonuniform illumination, two situations can occur: The first case occurs when the first row is shaded and the other rows are unshaded. In this case, the voltage of the first row is reduced, and it is less than the threshold voltage, i.e., $V_1 < \delta V$, and the adaptive reconfiguration starts. The second case occurs when the first row is unshaded and at least one of the other rows is shaded; the output voltage of the solar array is not equal to $m \times V_1$ but is much less than that, i.e., $V_{\text{out}} - (m-1) \times V_1 < \delta V$. In this case also, the adaptive reconfiguration starts.

Step 2) By opening all the switches, i.e., $S(1,1)$, $S(2,2),\ldots,S(m,m)$, all the solar cells in the solar adaptive bank are in the open circuits. Define and sort in a decreasing order the open-circuit voltages of all solar cells of the adaptive bank, i.e.,

$$V_{0A_1} > V_{0A_2} > \cdots > V_{0A_m}.$$

Step 3) Define the number of adaptive solar cells connected parallel to the shaded solar submodules in the fixed part.

Sorting: First, measure the voltages of all the submodules of the solar fixed part. Next, the voltages of all the submodules of the fixed part are sorted in an increasing order, i.e., $V_1 < V_2 < \cdots < V_m$—the voltages of the fixed part. Thus, the rows of the fixed part and each adaptive solar cell have been renumbered according their sorting voltages.

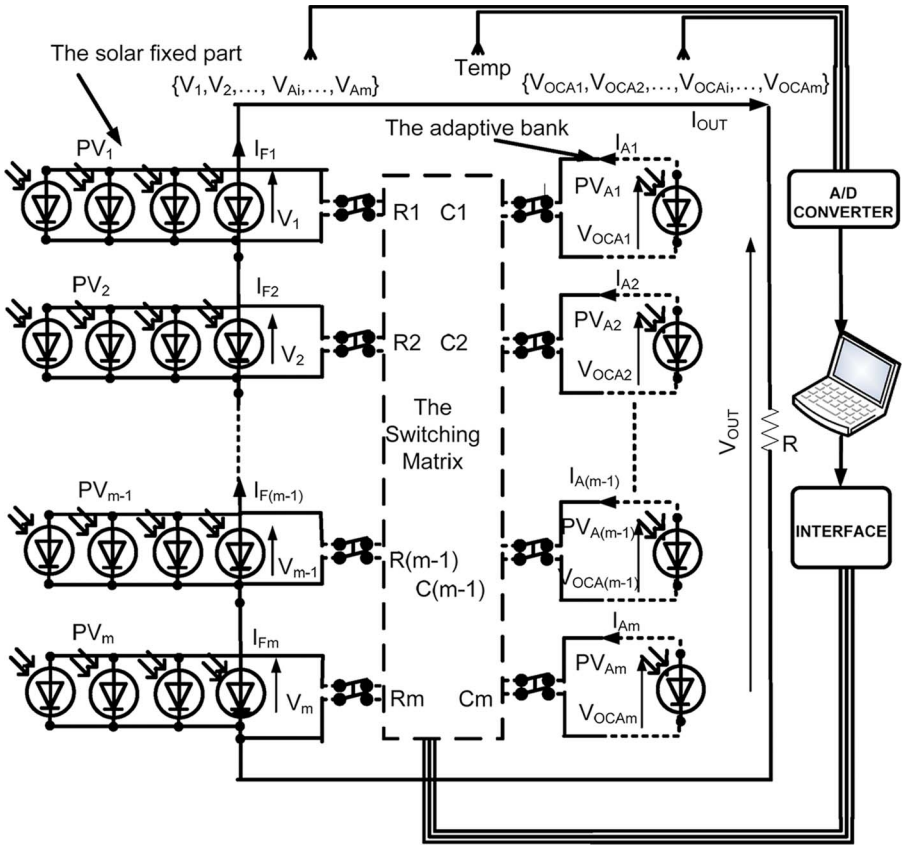

Fig. 6. Practical circuit of the proposed reconfiguration. For m rows in the fixed solar array, we proposed m solar cells in the adaptive bank.

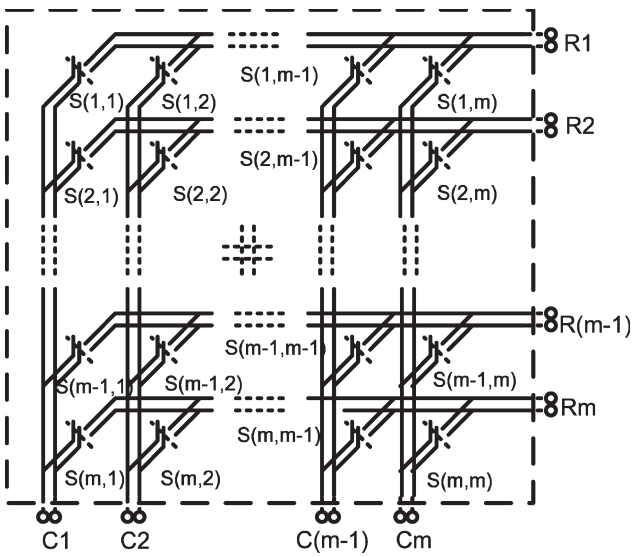

Fig. 7. Switching matrix.

Adding: Connect the solar cell with the maximum open-circuit voltage of the solar adaptive bank in parallel to the most shaded submodule of the fixed part, which has the smallest voltage. For example, if we switch solar cell A_1 in parallel with the submodule in row 1, then after the first switching, the solar adaptive bank becomes

$$V_{0A_2} > V_{0A_3} > \cdots > V_{0A_m}.$$

The fixed part might become

$$V_2 < V_1 < \cdots < V_m.$$

Then, the second switching occurs, and solar cell A_2 is connected in parallel with the submodule in row 2. We continue the reconfiguration process until all the solar cells of the solar adaptive bank are connected parallel to the rows of the fixed part.

Step 4) When the shadow changes direction or shape, the voltage of the first row and the output voltage are continuously being measured and compared and give the command to repeat the reconfiguration process, if the difference between them is above the fixed range, the control circuit repeats the procedure in Steps 2 and 3.

Model-Based Method: The flowchart of the model-based method is shown in Fig. 8(b). The control algorithm to determine how to connect and reconfigure the solar cells is based on a model-based control method and contains the following steps.

Step 1) It is the same as Step 1 in the "bubble-sort" method.

Step 2) Define the photo-generated currents of all solar cells of the solar adaptive bank and of all the submodules of the fixed part.

We can use the model-based method to calculate the photo-generated currents in Step 3. The advantage of this approach over the previous method is it defines photo-generated currents of all solar cells of the solar adaptive bank and of all the submodules

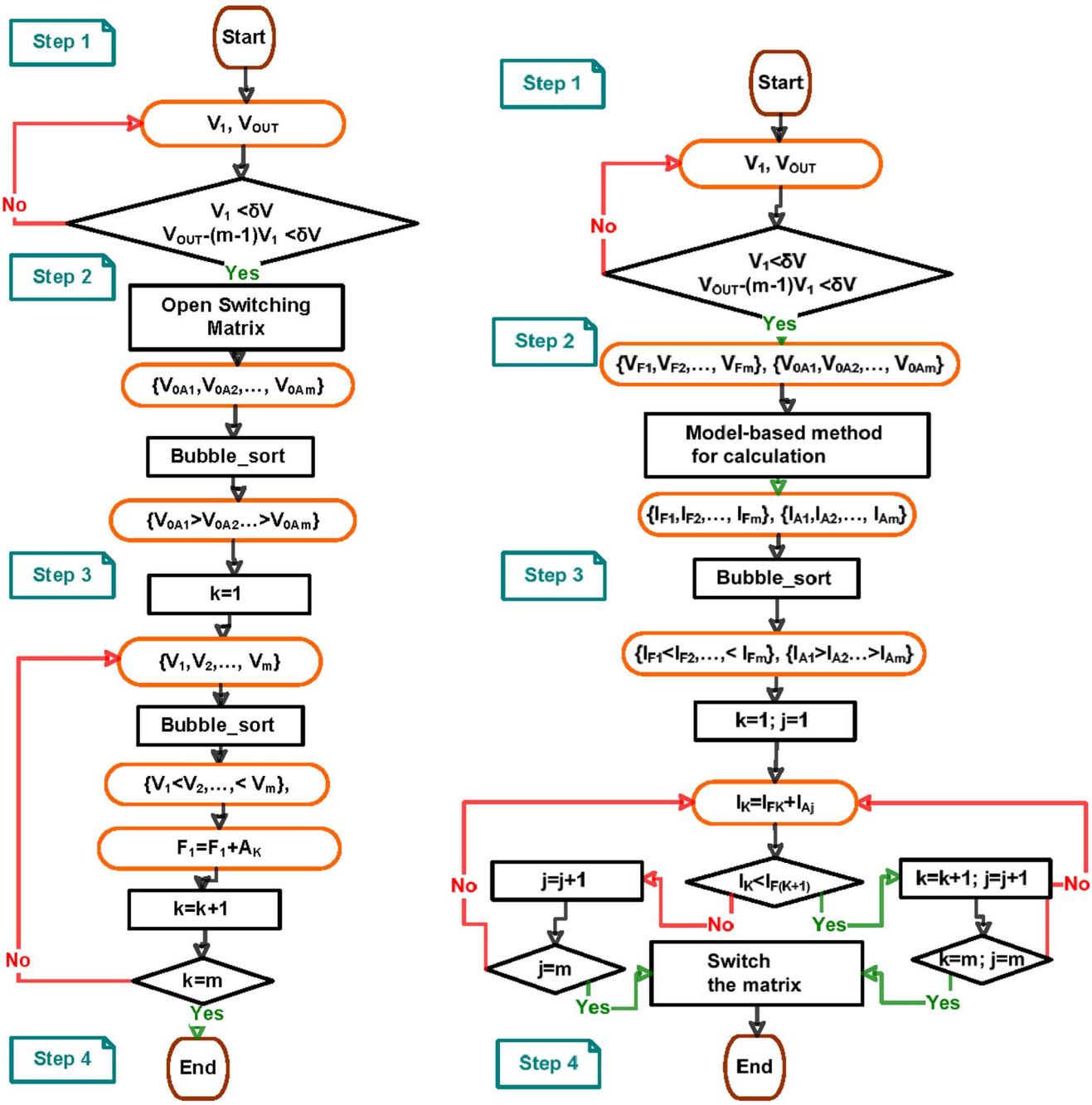

Fig. 8. Flowchart of the control algorithm. (a) "Bubble-sort" method. (b) Model-based method.

of the fixed part, and thus, all switches can be controlled synchronously at the same time.

The photo-generated currents of the solar adaptive bank: By the opening all the switches, i.e., $S(1,1), S(2,2), \ldots, S(m,m)$, all the solar cells in the solar adaptive bank are in the open circuits. By measuring the open-circuit voltages of solar cells, namely, $\{V_{\mathrm{OCA}_1}, V_{\mathrm{OCA}_2}, \ldots, V_{\mathrm{OCA}_m}\}$, the photo-generated currents I_{A_j} are estimated by the following equation:

$$I_{A_j} = \frac{V_{\mathrm{OCA}_j}}{R_{\mathrm{SH}}} + I_S^* \left(\exp\left(\frac{qV_{\mathrm{OCA}_j}}{akT} \right) - 1 \right). \quad (6)$$

Here, R_{SH} is the shunt resistance of solar cell (submodule), and I_S is the saturation current of the solar cell.

The photo-generated currents of the fixed part: All submodules of the fixed part are still working with load. Their photo-generated currents are calculated by

$$I_{F_j} = I_{\mathrm{out}} + nI_S \left[\exp\left(\frac{q}{akT}(V_j + I_{\mathrm{out}} R_{\mathrm{SM}}) \right) - 1 \right] + \left(\frac{V_j + I_{\mathrm{out}} R_{\mathrm{SM}}}{R_{\mathrm{SHM}}} \right) \quad (7)$$

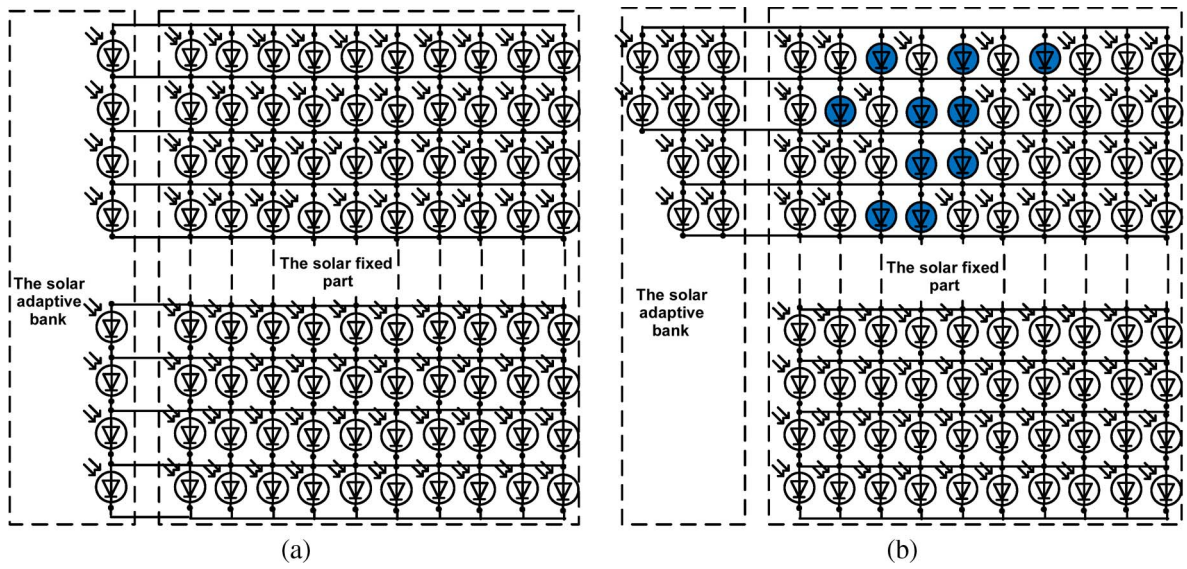

Fig. 9. Solar array's reconfiguration under nonuniform illumination. (a) Before configuration. (b) After reconfiguration.

where $\mathrm{V}_j = \{V_1, V_2, \ldots, V_m\}$ are the measured voltages of the submodules, I_{out} is the output current of the solar array, R_{SM} is the series resistance of the solar cell (submodule), R_{SHM} is the shunt resistance of the solar cell (submodule), I_S is the saturation current of the solar cell diode, and n is the number of solar cells in the submodule. These parameters of the solar cell or the solar submodule are received from manufacturers or are extracted based on experiments by V–I curve fitting [17]. By updating the temperature and voltage parameters in the model (in real time), it is possible to estimate the photo-generated currents I_{A_j} and I_{F_j} of each solar cell or submodule by using [18]–[20] and their dynamics multiphysics models [21].

Step 3) Define the number of adaptive solar cells connected parallel to the shaded solar submodules in the fixed part.

Sorting: First, the photo-generated currents of all the solar cells of the solar adaptive bank are defined and sorted in a decreasing order, i.e., $I_{A_1} > I_{A_2} > \cdots > I_{A_m}$—the current of the adaptive bank.

Next, the photo-generated currents of all the submodules of the fixed part are sorted in an increasing order, i.e., $I_{F_1} < I_{F_2} < \cdots < I_{F_m}$—the currents of the fixed part.

Thus, the rows of the fixed part and each adaptive solar cell have been renumbered according their sorting predicted photo-generated current.

Adding: Connect the solar cell with the maximum predicted photo-generated current of the solar adaptive bank in parallel to the most shaded submodule of the fixed part. For example, if we switch solar cell A_1 in parallel with the submodule in row 1, then after the first switching, the solar adaptive bank becomes $I_{A_2} > I_{A_3} > \cdots > I_{A_m}$.

The fixed part might become

$$I_{F_2} < I_{F_1} + I_{A_1} < \cdots < I_{F_m}.$$

Then, the second switching occurs, and solar cell A_2 is connected in parallel with the submodule in row 2. We continue the reconfiguration process until all the solar cells of the solar adaptive bank are connected parallel to the rows of the fixed part.

Step 4) When the shadow changes direction or shape, the voltage of the first row and the output voltage are continuously being measured and compared and give the command to repeat the reconfiguration process. If the difference between them is above the fixed range, the control circuit repeats the procedure in Steps 2 and 3.

Table I compares the previous reconfiguration structures [15], [16] with the proposed method. In the previous reconfiguration approaches, it is assumed that all solar cells are "adaptive," that is, that they can all be reconfigured to each other. In our proposed approach, we assume that there is a fixed array, and that this array has m rows and n columns of solar cells. Often, the number of columns is made greater than the number of rows, as the currents in each columns are added together to increase power.

Notice that the proposed method always uses fewer sensors, and in the case when the number of columns is significantly greater than the number of rows $(n > m)$, as it commonly occurs, then there are significantly fewer sensors. Similarly, when $n > m$, the number of switches can also be significantly decreased.

We remark that [15] and [16] do not present methodologies to determine how to reconfigure the solar arrays. Thus, we are unable to make comparisons in control algorithms.

One example of the reconfiguration method is shown in Fig. 9. The solar PV array from 10×10 solar cells in the fixed part, and ten solar cells in the adaptive part, has the

TABLE I
COMPARISON OF THE RECONFIGURATION METHODS

No	Item	Conventional	Proposed
1	Number of solar cells(submodules)	Fixed: 0 Adaptive: m(n+1)	Fixed: m(n) Adaptive: m
2	Number of voltage + current sensors	m(n+1)	2m+1
3	Number of switches	2m(n+1) to 3m(n+1)	$2m^2$
4	Control Algorithms	N/A	Bubble - Sort Model-based

interconnection in Fig. 9(a), in the uniform illumination, and in Fig. 9(b), in the nonuniform illumination. The figures show that by using the proposed adaptive reconfiguration method, when the number of shaded solar cells is less than the number of solar cells in one row, the maximum power loss is at most equal to the power of one row. If there is no adaptive bank and TCT connection, then the shade would incur a reduction in the maximum output power (three rows) of up to 30%. With the adaptive bank, there is only a 10% reduction in power.

Fig. 10 shows the I–V curves and P–V curves for two PV modules connected in series before and after reconfiguration by the proposed method. In the operating lines b and c, the unshaded solar module PV_1 cannot generate the full power because the current of this module is limited by the current of the shaded module PV_2. Hence, for example, in operating line b, the unshaded PV_1 operates at I–V point Sb_1 and the shaded PV_2 operates at I–V point Sb_2. In series, the total array will operate at their voltage sum while at the same fixed current, i.e., operating point Sb.

In operating line a, the unshaded module PV_1 generates full power, but the operating point of the shaded module PV_2 moves to the negative region. PV_2 works as a load and causes losses in the system. The output power is decreased, i.e.,

$$P_{\text{out}} = P_{\text{out1}} - P_{\text{losses2}}. \tag{8}$$

From the above discussion, the main reason to cause the losses in the solar PV array is the fact that the currents of the series-connected solar cells or solar submodules are limited by the current of the shaded solar cell or the shaded solar submodule.

After reconfiguration, the operating point of the solar PV array moved from the point Sb in Fig. 10(a) to point Sbmax in Fig. 10(b). The maximum output power of the whole solar PV array increases from point PSb to PSbmax in Fig. 10(c).

IV. EXPERIMENT RESULT

Fig. 11 shows the solar PV array test platform. The experiment includes the following: The fixed solar array is from nine solar cells: three rows (m) and three columns (n) (TCT connection). The solar adaptive bank is from three solar cells (one string of 3×1 cells) connected to the fixed part (3×3). The 3×3 switching matrix, controlled by Agilent Data Acquisition/Switch Unit 34970A, is connected between the fixed part and the solar adaptive bank. In total, we use 18 switches in the switching matrix and six voltage sensors (two of them are voltage monitors) for this test platform. The output load in all the experiments is 10 Ω.

The voltages of solar cells in the solar adaptive bank and solar submodules in the fixed part are continuously measured and sent to a PC running real-time MATLAB software. The sorting algorithm previously described is implemented by the PC in real-time.

Bubble-Sort Method: Fig. 12(a) shows two separate experiments: Experiment 1 is for $0 < t < T_3$. In this time interval, the figure shows the output voltage of the solar array when four solar cells are *partially shaded*. From time 0 to T_1, the output voltage is under uniform illumination. From T_1, the solar PV array is shaded. The interval T_1–T_2 is the time for measurement and control. After T_3, the output voltage of the solar array has been optimized, and the reconfiguration has been completed. Notice that from T_3 to T_4, clouds move across the array and cause a change in the output voltage. However, no reconfiguration occurs since the clouds affect both the adaptive and fixed part of the solar array equally. Hence, this demonstrates a robustness of the proposed algorithms to falsely reconfigure when it is not necessary.

The output power of the solar PV array is calculated by the following equation:

$$P_{\text{out}} = \frac{V_{\text{out}}^2}{R}. \tag{9}$$

For experiment 1, there is a 62.3% increase in output power from before to after the reconfiguration.

Experiment 2 of the bubble-sort method is performed at $t > T_4$ in Fig. 12(a). At $t < T_4$, the solar system is in the configuration stage from experiment 1. All of a sudden, at $t = T_4$, the shadow configuration is suddenly changed so that two cells in the same row of the fixed part are *fully shaded*. The interval T_4–T_5 is the time for measurement and control. After T_6, the output voltage of the solar array has been optimized, and the bubble-sort reconfiguration has been completed. Using the data in Fig. 12(a) with (9), it is calculated that there is a 156% increase in output power from before to after the reconfiguration.

In both experiments, the bubble-sort reconfiguration takes about 18 s.

Model-Based Method: Fig. 12(b) shows two more experiments. Experiment 3 is for $0 < t < T_2$, and experiment 4 is for $t > T3$. In experiment 3, the output voltage of the solar array when four solar cells are *partially shaded* is shown in the figure. From 0 to T_1, the output voltage is under uniform illumination. From T_1, the solar PV array is shaded. The interval T_1–T_2

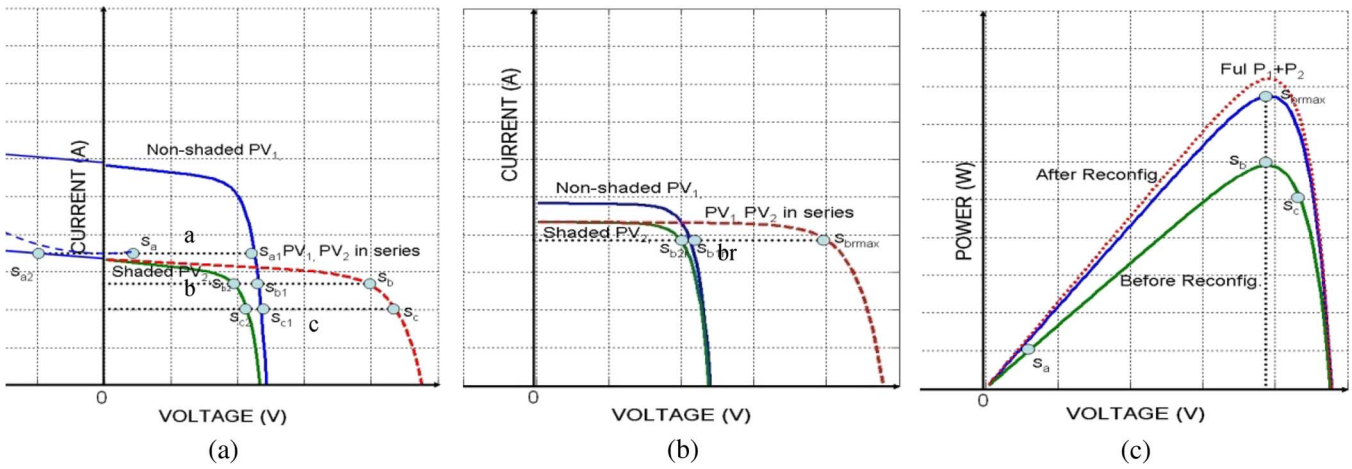

Fig. 10. I–V and P–V curves before and after reconfiguration. (a) I–V curve before configuration. (b) I–V curve after reconfiguration. (c) P–V curves.

Fig. 11. Solar PV array outdoor test platform.

is the time for measurement and control. After T_2, the output voltage of the solar array increases after reconfiguration. Notice that the voltage across the load is increased from T_2 by 20%, indicating a 33% increase in power due to reconfiguration. The output voltage of solar array initially drops during real time reconfiguration (between T_1 and T_2). This is because the solar adaptive bank is disconnected from the load for a short time to measure and sort. During the transition, though, the fixed part is still supplying power for the load.

In experiment 4, as shown in Fig. 12(b) for $t > T_3$, the shadow configuration suddenly changes so that three solar cells in the fixed part are completely shaded. The three solar cells in the adaptive bank remain illuminated. The reconfiguration starts at $t = T_3$ from the previous reconfiguration connections of experiment 3, but this provides no technical difficulties. From T_3 to T_4, there is measurement and control. After T_4, the switches are controlled synchronously to reconfigure. For this experiment, the reconfiguration from T_3 to T_4 led to dramatic increases of power from before to after reconfiguration—a 3900% improvement.

Comparison Between the "Bubble-Sort" Method and the Second Method: The second reconfiguration method takes about 8 s. This method is faster because all switches can be controlled synchronously at the same time, when the "bubble-sort" method switches one at a time instead of all at once. The final reconfiguration state does not differ between the two methods.

Partly Shaded Solar Adaptive Bank: At times, one can expect that the adaptive solar cells may also become shaded. As previously discussed, all the algorithms work when this occurs. For the case when there are still more illuminated adaptive solar cells than shaded fixed solar cells, there will still be significant power improvements after reconfiguration. Fig. 13(a) shows the output voltage of the solar cells when two fixed solar cells and one adaptive solar cell are fully shaded. (Thus, there are still two adaptive solar cells that are fully illuminated.) As in the previous two experiments, from 0 to T_1, the output voltage is under uniform illumination. After T_1, two fixed solar cells in the same row and one adaptive solar cell are fully shaded. The interval T_1-T_2 is the time for measurement and control. At T_2, three illuminated adaptive solar cells are connected in parallel with the shaded row at the same time. Using the data in Fig. 13(a), with (9), it is calculated that there is a 65% increase in output power from before to after the reconfiguration.

The Number of Shaded Fixed Solar Cells is Larger Than the Number of Solar Adaptive Banks: It is possible that many adaptive solar cells become shaded, and that there will not be a sufficient number of them to compensate for all the shaded solar cells in the fixed part.

Alternatively, this could also occur if fewer adaptive solar cells are used, as we are only recommending "m" number of adaptive cells. Still, there is a benefit from the reconfiguration algorithms adding power to the system, and both reconfiguration algorithms will still work. Of course, less power can be added to the system.

Fig. 13(b) shows the output voltage of the solar cells when four fixed solar cells are *fully shaded*, three of which are in the same row. There remain three fully illuminated adaptive solar cells.

From 0 to T_1, the output voltage is under uniform illumination. After T_1, four fixed solar cells in the same row are fully shaded. The interval T_1-T_2 is the time for measurement and control. At T_2, three illuminated adaptive solar cells are connected in parallel with the shaded row all at the same time. For this experiment, the reconfiguration from T_1 to T_2 led to dramatic increases of power from before to after reconfiguration—a 4125% improvement.

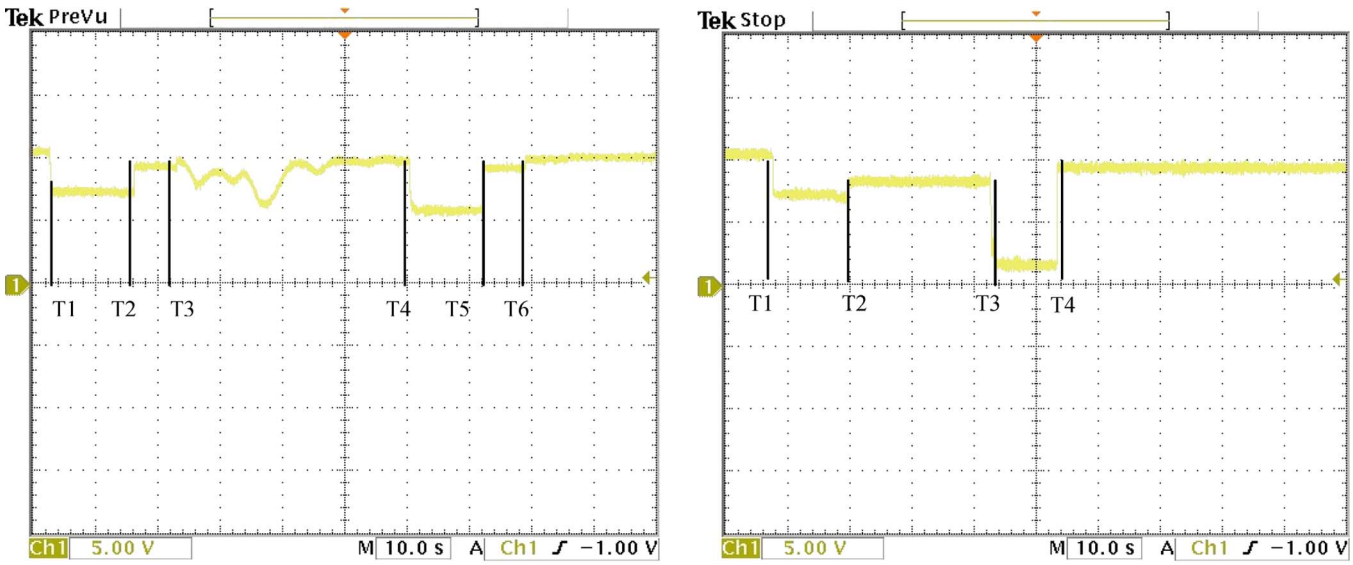

Fig. 12. Output voltage of a solar PV array before and after reconfiguration. (a) Two bubble-sort experiments. (b) Two model-based experiments.

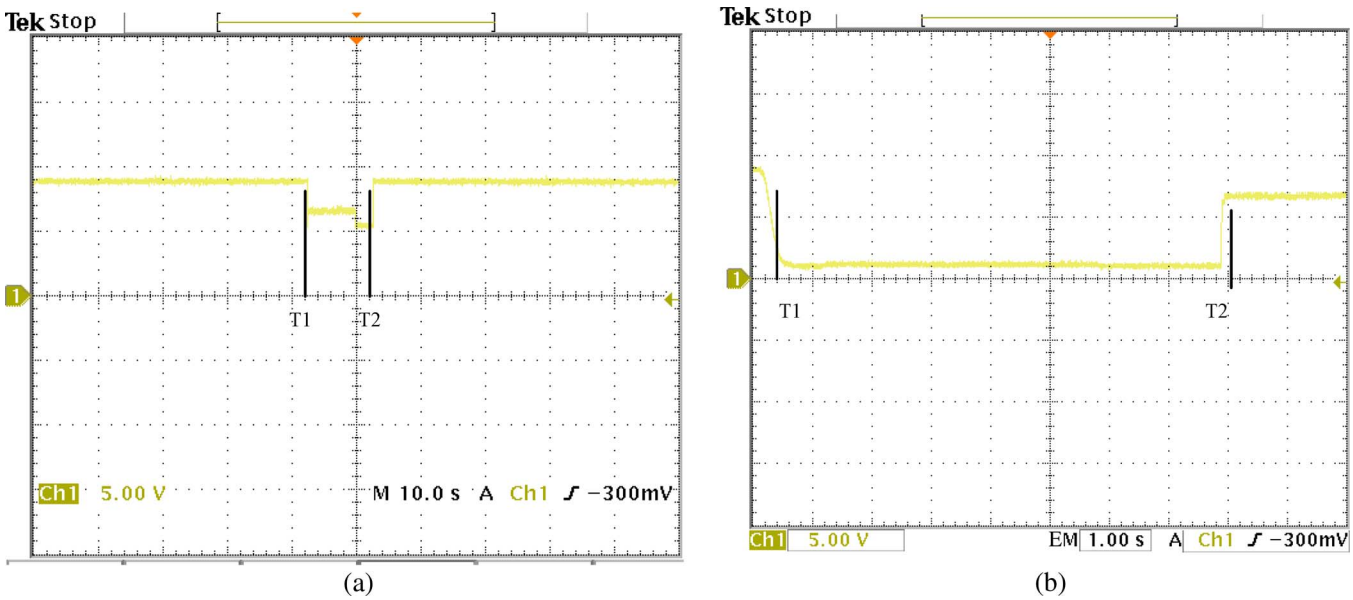

Fig. 13. Output voltage of a solar PV array. (a) Partly shaded solar adaptive bank. (b) Number of shaded fixed solar cells is larger than the number of solar adaptive banks.

V. Conclusion

A new approach for adaptive reconfiguration of solar PV arrays under shadow conditions has been described. A matrix of switches is used to connect a "fixed" TCT array with an adaptive array that can be reconfigured. Simple control algorithms that determine how the switches can be controlled to optimize output power are presented. An experimental adaptively reconfigurable solar PV array has been built and tested to verify the proposed configurations.

The switching matrix may still require a large number of switches, and this represents a disadvantage of the approach. However, we show that when the number of rows in the solar array is not too large, the number of switches and sensors is significantly reduced. Further, we present four separate experiments that demonstrate the technical feasibility of two different reconfiguration algorithms. The reconfiguration methods are shown to be effective in improving solar array power, even when the number of shaded arrays is more than the power provided by the adaptive solar modules to be switched into the system. The model-based sorting algorithms have reduced calculation time.

Acknowledgment

The opinions, findings, and conclusions stated herein are those of the authors and do not necessarily reflect those of VEF.

REFERENCES

[1] F. Jeffrey, Power Film Inc., private communication.

[2] H. S. Raushenbach, "Electrical output of shadowed solar arrays," *IEEE Trans. Electron Devices*, vol. 18, no. 8, pp. 483–490, Aug. 1971.

[3] V. Quaschning and R. Hanitsch, "Influence of shading on electrical parameters of solar cells," in *Proc. IEEE Photovolt. Spec. Conf.*, May 13–17, 1996, pp. 1287–1290.

[4] D. Weinstock and J. Appelbaum, "Shadow variation on photovoltaic collectors in a solar field," in *Proc. 23rd IEEE Conv. Electr. Electron. Eng.*, 2004, pp. 354–357.

[5] D. Weinstock and J. Appelbaum, "Optimal design of solar fields," in *Proc. 22nd Conv. Electr. Electron. Eng.*, 2002, pp. 163–165.

[6] W. T. Jewell and T. D. Unruh, "Limits on cloud-induced fluctuation in photovoltaic generation," *IEEE Trans. Energy Convers.*, vol. 5, no. 1, pp. 8–14, Mar. 1990.

[7] M. S. Swaleh and M. A. Green, "Effect of shunt resistance and bypass diodes on the shadow tolerance of solar cell modules," *Sol. Cells*, vol. 5, no. 2, pp. 183–198, Jan. 1982.

[8] N. F. Shephard and R. S. Sugimura, "The integration of bypass diodes with terrestrial photovoltaic modules and arrays," in *Proc. 17th IEEE Photovolt. Spec. Conf.*, 1984, pp. 676–681.

[9] T. Shimizu, M. Hirakata, T. Kamezawa, and H. Watanabe, "Generation control circuit for photovoltaic modules," *IEEE Trans. Power Electron.*, vol. 16, no. 3, pp. 293–300, May 2001.

[10] W. Xiao, N. Ozog, and W. G. Dunford, "Topology study of photovoltaic interface for maximum power point tracking," *IEEE Trans. Ind. Electron.*, vol. 54, no. 3, pp. 1696–1704, Jun. 2007.

[11] K. Kobayashi, H. Matsuo, and Y. Sekine, "Novel solar-cell power supply system using a multiple-input DC–DC converter," *IEEE Trans. Ind. Electron.*, vol. 53, no. 1, pp. 281–286, Feb. 2006.

[12] E. Roman, P. Ibanez, S. Elorduizapatarietxe, R. Alonso, D. Goitia, and D. A. Martinez, "Intelligent PV module for grid-connected PV systems," *IEEE Trans. Ind. Electron.*, vol. 53, no. 4, pp. 1066–1073, Jun. 2006.

[13] M. A. El-Shibini and H. H. Rakha, "Maximum power point tracking technique," in *Proc. Electrotech. Conf., MELECON*, Apr. 11–13, 1989, pp. 21–24.

[14] Y. Auttawaitkul, B. Pungsiri, K. Chammongthai, and M. Okuda, "A method of appropriate electrical array reconfiguration management for photovoltaic powered car," in *Proc. IEEE Asia-Pacific Conf. Circuit Syst.*, 1998, pp. 201–204.

[15] C. Chang, "Solar cell array having lattice or matrix structure and method of arranging solar cells and panels," U.S. Patent 6 635 817, Oct. 21, 2003.

[16] R. A. Sherif and K. S. Boutros, "Solar module array with reconfigurable tile," U.S. Patent 6 350 944, Feb. 26, 2002.

[17] W. Durisch and J.-C. Mayor, "Application of a generalized current/voltage model for solar cells to outdoor measurements on a Siemen SM 110-module," in *Proc. 3rd World Conf. Photovolt. Energy Convers.*, May 12–16, 2003, pp. 1956–1959.

[18] V. Quaschning and R. Hanitsch, "Numerical simulation of current–voltage characteristics of photovoltaic systems with shaded solar cells," *Sol. Energy*, vol. 56, no. 6, pp. 513–520, Jun. 1996.

[19] N. D. Kaushika and N. K. Gautam, "Energy yield simulations of interconnected solar PV arrays," *IEEE Trans. Energy Convers.*, vol. 18, no. 1, pp. 127–134, Mar. 2003.

[20] D. D. Nguyen and B. Lehman, "Modeling and simulation of solar PV arrays under changing illumination conditions," in *Proc. IEEE COMPEL*, Jul. 16–19, 2006, pp. 295–299.

[21] S. Liu and R. A. Dougal, "Dynamic multiphysics model for solar array," *IEEE Trans. Energy Convers.*, vol. 17, no. 2, pp. 285–294, Jun. 2002.

Dzung Nguyen (S'07) was born in Hanoi, Vietnam. He received the M.S. degree in electrical engineering from Kiev Polytechnic Institute, Kiev, Ukraine, in 1993. He is a Vietnam Education Foundation Fellow and is currently working toward the Ph.D. degree in electrical engineering at Northeastern University, Boston, MA.

His research interests include photovoltaic systems and dc–dc converters.

Brad Lehman (M'92) received the B. and Ph.D. degrees in electrical engineering from Georgia Institute of Technology, Atlanta, in 1987 and 1992, respectively, and the M.S. degree in electrical engineering from the University of Illinois, Urbana, in 1988.

He was a Hearin Hess Distinguished Assistant Professor with Mississippi State University. He is currently a Professor with the Department of Electrical and Computer Engineering, Northeastern University, Boston, MA. He was a Visiting Scientist with the Massachusetts Institute of Technology, Cambridge. He performs research in the areas of power electronics, with primary focus on the modeling, design, and control of dc–dc converters with applications to high-brightness LEDs, battery chargers, telecommunication power supplies, and VRMs.

Dr. Lehman was a National Science Foundation Presidential Faculty Fellow. He was a recipient of an Alcoa Science Foundation Fellowship. He serves as an Associate Editor for the IEEE TRANSACTIONS ON POWER ELECTRONICS. From 1993 to 1997, he served as an Associate Editor for the IEEE TRANSACTIONS ON AUTOMATIC CONTROL. In 1999, he served as a Science Advisor to the Commonwealth of Massachusetts, Science and Technology Committee (State Senate), for the Y2K issue in the power industry.